Jamming-Free Immobilizing Grasps Using Dual-Friction Robotic Fingertips

Yoav Golan, Amir Shapiro, and Elon Rimon

***Abstract*—Successful grasping of objects with robotic hands is still considered a difficult task. One aspect of the grasping problem is the physical contact interaction between the robotic fingertips and the object. Friction at the fingertip contacts can improve grasp robustness, but frictional fingertips may be difficult to precisely place on the object's perimeter. This paper describes a novel fingertip design that can switch from frictionless to frictional modes. The transformation from frictionless to frictional contact is achieved passively by the finger force exerted on the object at the target grasp. A novel swivel mechanism ensures that the force magnitude required to switch friction states is independent on the grasped object's contact normal direction, thus ensuring robustness. Analysis of the displacement and eventual sliding of the fingertip contacts in response to external torque is presented, taking into account the amount of friction and the compliant behavior of the fingertip mechanism. Experiments validate the analytic model and demonstrate the fingertip's ability to change friction modes by the applied force magnitude irrespective of the contact normal direction. In line with the analytic model predictions, the experiments show that when converted to frictional contacts, the fingertips provide a more robust and hence secure grasp in the presence of external disturbances. The robustness of the fingertips is further validated by real-world demonstrations shown in an external video referenced in the paper.**

***Index Terms*—Grasping, mechanism design, contact modeling.**

I. Introduction

WHEN ATTEMPTING to grasp objects with a robotic hand, the success or failure of the grasping task relies on the fingertip contacts with the object. Well placed, suitable contact points will allow the application of forces required to properly manipulate an object or use a tool even in uncertain conditions. However, we do not usually have the luxury of designing robotic hands and fingers to fit a specific task. Instead, we typically attempt to design generic robot hands that can perform a wide variety of tasks, albeit not optimally. A challenge in developing general-use robotic hands is making them as simple as possible while retaining good grasping capability. This trend of simplification was recognized by Bicchi [1], Dollar *et al.* [2], Rodriguez *et al.* [3], and Xiong *et al.* [4]. Minimalistic robotic hand design requires out-of-the-box solutions to provide enhanced capabilities with simple operational principles. For instance, some researchers have advocated the use of compliance [5], while others have focused on securing grasps without friction [6], [7]. Research has also been done on searching for optimal contact locations on a case-to-case basis with or without friction [8], [9]. Grasp selection often relies on quantification of grasp quality, commonly measured as the robustness of the grasp against external disturbances [10], [11].

In an effort to design minimalistic robot hands, this paper focuses on the dual role of frictionless and frictional contacts in achieving reliable robotic grasps. In general, frictional grasps are more robust than frictionless ones. On the other hand, frictionless contacts allow precise placement of the finger contacts at a target grasp. By initially placing the fingers in a caging formation, the cage can be closed until the object is *immobilized* at predictable contact points. This type of grasp is highly secure based on pure rigid body constraints. Conversely, if a set of frictional fingertips are retracted upon an object from a caging position, the result will be a frictional *jamming grasp* whose precise location is not predictable. Moreover, such grasps are susceptible to small perturbations that can dislodge the object from the jammed state in a stick-slip manner. Frictionless contacts thus have the advantage of allowing precise grasping, while frictional contacts are more robust given the same contact locations. Ideally, we can utilize both advantages to gain grasp robustness. Once a secure immobilizing grasp is established using frictionless contacts, a switch to frictional contacts permits enhanced grasp robustness against external disturbances.

Observe Fig. 2 as an example. Three fingers are used to grasp an object, in this case a "fidget spinner" toy. In subfigures (a–c) the fingers have high-friction (marked as orange discs). When retracting upon the object under frictional contact conditions, two of the three fingers will typically reach an undesirable jamming grasp, as shown in subfigure (b). When an external torque is applied in subfigure (c), the jamming grasp may be compromised, even resulting in a loss of grip on the object. In subfigures (d-f) the fingers have no friction (marked as green discs). While retracting upon the object, the sliding contacts will impose displacement and reorientation of the object until a secure three-finger immobilizing grasp is achieved. However, when an external torque is applied in subfigure (f), the fingers slide along the object perimeter due to their natural compliance. In subfigures (g-i) the fingers have changeable friction. The fingers retract as frictionless contacts (subfigure (g)), displacing the object until grasped, identically to (e). Once the grasp is reached, the contacts are turned to high-friction contacts (subfigure (h)).

Manuscript received September 10, 2019; accepted January 27, 2020. Date of publication February 10, 2020; date of current version February 27, 2020. This letter was recommended for publication by Associate Editor Dr. A. Morales, Editor Prof. H. Liu, Allison M. Okamura and H. Ding upon evaluation of the reviewers' comments. This work was supported by the Israel Science Foundation under Grant 1253/14 and in part by the Helmsley Charitable Trust through the Agricultural, Biological and Cognitive Robotics Center of Ben-Gurion University. *(Corresponding author: Yoav Golan.)*

Yoav Golan and Amir Shapiro are with the Department of ME, Ben-Gurion University of the Negev, Tel Aviv 6219403, Israel (e-mail: yoavgo@post.bgu.ac.il; ashapiro@bgu.ac.il).

Elon Rimon is with the Department of ME, Technion - Israel Instit. of Technology, Haifa 32000, Israel (e-mail: rimon@technion.ac.il).

Digital Object Identifier 10.1109/LRA.2020.2972883

2377-3766 © 2020 IEEE. Personal use is permitted, but republication/redistribution requires IEEE permission.
See https://www.ieee.org/publications/rights/index.html for more information.

Authorized licensed use limited to: Ben-Gurion University of the Negev. Downloaded on December 03,2023 at 08:12:58 UTC from IEEE Xplore. Restrictions apply.

When an external torque is applied in subfigure (i), the fingers roll and possible slide along the object's perimeter due to their natural compliance. This is similar to the frictionless case in (f), but to a much lesser extent, thanks to the frictional contacts. In terms of grasp robustness and fingertip displacement, the best result is achieved by the dual-friction fingertips.

This paper seeks to exploit the advantages of both frictionless and frictional contacts in a single robotic fingertip design. Such focus on fingertip design is not new. Takeuchi and Watanabe [12] developed robotic fingertips with softness-changeable skin by electro-chemical stimulation. Spiers *et al.* [13] recently introduced robotic fingertips that use an internal motor to change their contact surface characteristics from low to high-friction. Both fingertips are designed primarily for in-hand manipulation tasks. Our paper complements these works with a completely different design approach to utilize the alteration of friction to improve grasping. Our novel robotic fingertip realizes a true frictionless contact when the fingertips close on an object, then realizes a high-friction contact when the desired grasp is achieved. Other works have changed friction by using actuated methods such as electroadhesion [14], ultrasonic vibration [15] and other means. In our case the transformation is done purely with passive mechanical means, without any actuators in the gripping system. Our fingertips change their friction in a binary manner, triggered by a contact force that meets an adjustable magnitude threshold at the immobilizing grasp. Moreover, this contact force threshold is independent of the object-fingertip interaction geometry. Our dual-friction fingertips were first presented at a workshop on exploiting contact and dynamics in manipulation [16], and have since been patented [17].

Before presenting the dual-friction finger design in Section III, we first present an analysis of the robustness advantage when using friction vs. frictionless contacts, in Section II. This analysis will serve as motivation for the use of dual-friction fingers, predicting the improvement of robustness when using high-friction contacts. However, this analysis also stands as a contribution in and of itself, by examining contact dynamics with natural compliance, rolling and sliding. It is important to note that the analysis is not yet generalized to arbitrary cases and is used here primarily to gain intuition on the contribution of our dual-friction fingertips. The robustness parameter we analyze is the displacement of the fingertip contacts from their grasping points when an external torque disturbance is applied to the grasped object. We show that the displacement of the fingertip contacts is *significantly lower* when friction is present. The analytic model takes into account the compliant nature of the fingertip mechanism, and demonstrates the relative advantages of switching from frictionless to frictional contacts once a desired immobilizing grasp is achieved.

In the following section, we describe the design of our dual-friction robotic fingertips, including three of its key features– the frictionless to high-friction locking mechanism, contact force direction normalization, and locking force adjustment. Section IV describes experiments performed that validate both the theoretical analysis in a real world setting, and the key finger design principles. Firstly, the analysis of finger displacement is validated by replicating the case study in Section II with frictionless and frictional fingertips. Secondly, the dual-friction fingertips's normalization mechanism is verified by applying contact forces from different directions and testing the response. Section V concludes with a discussion of future work. Although experiments on real-world objects are beyond the scope of this paper, we also provide a comprehensive video of grasping demonstrations using our fingertips in [18]. This video demonstrates how grasping various objects using the presented dual-friction fingertips is more robust than other types of fingertips.

II. The Advantage of Friction Contacts

This section analyzes a case study where the contacts of a grasp switch from frictionless to frictional conditions. Our objective would be to demonstrate how the switch from frictionless to frictional contact conditions *increases grasp robustness* against external disturbances. We will show that the presence of friction has a quantifiable, positive contribution to grasp robustness. Specifically, that using friction drastically reduces the displacement of the fingertip contacts when external wrenches are applied to a grasped object.

In this case study, a three-finger robotic hand having disc-shaped fingertips grasps a rigid equilateral triangle $\mathcal{B}$. The hand keeps the three disc fingers equidistant at points located on the inscribed circle of $\mathcal{B}$ (Fig. 3(a)). This grasp is immobilizing and hence secure [19]. Such three-finger hands can in fact immobilize every polygonal object which does not possess opposing parallel edges [20].

While this grasp is immobilizing based on rigid body constraints, our fingertips possess compliance due to their internal structure. Hence, external wrenches that act on $\mathcal{B}$ will displace the fingertip contacts from their locations at the initial grasp, while stressing the fingertip internal structure. We model the fingertip compliance in terms of mutually orthogonal *linear springs*; one normal to the object edge, the other tangent to the object edge at the initial grasp (Fig. 3(a)). Once friction is switched on, the fingertips may also roll when the object is perturbed, and their rolling compliance is modeled by a *torsional spring*. The torsional spring forms part of the disc-shaped fingertip and rotates about its center (Fig. 3(a)), while the disc center is attached to the linear springs. Let τ_{ext} be an external torque applied to $\mathcal{B}$ at its center (which forms the grasp center of compliance). Let ρ denote the displacement of a fingertip contact from its initial contact along the object's perimeter. Note that the displacement of each fingertip contact is identical due to symmetry. We now seek to find a relation between ρ and τ_{ext} under different friction conditions. In order to find the $\rho(\tau_{\text{ext}})$ relation, we assume:

- The rigid object $\mathcal{B}$ rotates by an angle θ about its center when τ_{ext} is applied (Fig. 3(b)).
- All three fingers respond identically. Therefore from this point onward, the analysis will focus on the bottom finger (Fig. 3(a)).
- At the initial grasp, a normal force of magnitude f_0^n is applied by the finger due to precompression of the linear spring in the y-direction.
- The fingertip-object coefficient of friction is μ.
- The stiffness coefficients of the linear springs in the x and y directions are k_x and k_y.
- The stiffness coefficient of the torsional spring is k_ψ.
- The radius of the disc-shaped fingertip is r, the radius of the object's inscribed circle is R.
- The rotation of a reference frame attached to the the disc fingertip center relative to the world frame is ψ.
- The rotation of the disc fingertip relative to $\mathcal{B}$'s reference frame is ϕ.

Authorized licensed use limited to: Ben-Gurion University of the Negev. Downloaded on December 03,2023 at 08:12:58 UTC from IEEE Xplore. Restrictions apply.

The world frame is placed at the center of $\mathcal{B}$, and is coincident with $\mathcal{B}$'s frame when $\tau_{\text{ext}} = 0$. The initial contact point of the bottom finger is:

$$\vec{x}_0 = \vec{b}_0 = \begin{pmatrix} 0 \\ -R \end{pmatrix} \tag{1}$$

where $\vec{x}_0$ is the contact location in the world frame, and $\vec{b}_0$ is the contact location in $\mathcal{B}$'s frame.

After an external torque τ_{ext} is applied, the fingertip contact location moves to a new equilibrium at:

$$\vec{x}_1 = R(\theta)\vec{b}_1 + \vec{d} \tag{2}$$

where $\vec{x}_1$ is the new contact location in the world frame, $\vec{b}_1$ is the new contact in $\mathcal{B}$'s frame, $\vec{d}$ is the translation of $\mathcal{B}$'s frame relative to the world frame and $R(\theta) = \left[\begin{smallmatrix} \cos(\theta) & -\sin(\theta) \\ \sin(\theta) & \cos(\theta) \end{smallmatrix}\right]$.

The position of the new contact in $\mathcal{B}$'s frame is

$$\vec{b}_1 = \vec{b}_0 + \begin{pmatrix} \rho \\ 0 \end{pmatrix} = \begin{pmatrix} \rho \\ -R \end{pmatrix}. \tag{3}$$

The displacement of the contact point relative to its resting position at the initial grasp is:

$$\vec{x}_1 - \vec{x}_0 = \left(\begin{bmatrix} \cos(\theta) & -\sin(\theta) \\ \sin(\theta) & \cos(\theta) \end{bmatrix} \begin{pmatrix} \rho \\ -R \end{pmatrix} + \vec{d} \right) - \begin{pmatrix} 0 \\ -R \end{pmatrix}. \tag{4}$$

Next, we find the position of the fingertip center. Since the finger is a disc of radius r, it's position at the initial grasp is:

$$\vec{p}_0 = \vec{x}_0 - \begin{pmatrix} 0 \\ r \end{pmatrix} = \begin{pmatrix} 0 \\ -R - r \end{pmatrix}, \tag{5}$$

and at the pertubed grasp

$$\begin{aligned} \vec{p}_1 &= \vec{x}_1 - R(\theta) \begin{pmatrix} 0 \\ r \end{pmatrix} \\ &= \begin{bmatrix} \cos(\theta) & -\sin(\theta) \\ \sin(\theta) & \cos(\theta) \end{bmatrix} \begin{pmatrix} \rho \\ -R - r \end{pmatrix} + \vec{d} \end{aligned} \tag{6}$$

The displacement of the fingertip center in the world frame is denoted $(\Delta x, \Delta y)$. It is as follows:

$$\begin{aligned} \begin{pmatrix} \Delta x \\ \Delta y \end{pmatrix} &= \vec{p}_1 - \vec{p}_0 \\ &= \begin{pmatrix} \cos(\theta)\rho + \sin(\theta)(R + r) \\ \sin(\theta)\rho - \cos(\theta)(R + r) \end{pmatrix} + \begin{pmatrix} 0 \\ R + r \end{pmatrix} + \vec{d}. \end{aligned} \tag{7}$$

The linear springs apply mutually orthogonal forces at the disc-fingertip center. The body $\mathcal{B}$ applies forces to the fingertip as well, balancing out the spring forces in static equilibrium under the influence of τ_{ext}. The force equilibrium on the fingertip is given by:

$$\begin{pmatrix} k_x(\Delta x + \Delta x_0) \\ k_y(\Delta y + \Delta y_0) \end{pmatrix} + R(\theta) \begin{pmatrix} f_t \\ f_n \end{pmatrix} = \vec{0} \tag{8}$$

where k_x, k_y are the spring stiffness coefficients, while f_t and f_n are the tangential and normal forces applied by $\mathcal{B}$ to the fingertip. Δx_0 and Δy_0 are the displacement of a fingertip in the x and y directions when $\tau_{\text{ext}} = 0$. In other words, $\Delta x_0, \Delta y_0$ represent the preloaded grasp spring's precompression. In our case study, when $\tau_{\text{ext}} = 0$, the bottom finger has a precompression in the y-direction $\Delta y_0 \neq 0$, and $\Delta x_0 = 0$, resulting in a non-zero normal force f_n^0 exerted on the body by the fingertip.

Based on Eq. (8), the contact force components are given by:

$$\begin{pmatrix} f_t \\ f_n \end{pmatrix} = -R(\theta)^T \begin{pmatrix} k_x(\Delta x + \Delta x_0) \\ k_y(\Delta y + \Delta y_0) \end{pmatrix} \tag{9}$$

Since $\Delta x_0 = 0$, By symmetry there is no net object displacement in response to τ_{ext}, therefore there is no object displacement, hence $\vec{d} = \vec{0}$. Substituting $\Delta x_0 = 0$, $\vec{d} = \vec{0}$, and $(\Delta x, \Delta y)$ according to Eq. (7) gives:

$$\begin{aligned} \begin{pmatrix} f_t \\ f_n \end{pmatrix} &= -R(\theta)^T \\ &\quad \times \begin{pmatrix} k_x\left(\cos(\theta)\rho + \sin(\theta)(R + r)\right) \\ k_y\left(\sin(\theta)\rho - (\cos(\theta) + 1)(R + r) + \Delta y_0\right) \end{pmatrix} \end{aligned} \tag{10}$$

Similarly to the force equilibrium analysis in (8), we can analyze the static equilibrium of the fingertip moments. The normal force f_n as well as the linear spring forces all pass through the disc-fingertip's center, and therefore do not apply moments about it. The only components of the moments are therefore generated by the tangential force, f_t, and the pure moment applied to the fingertip by the torsional spring due to rolling without slippage:

$$k_\psi \psi = f_t r \tag{11}$$

Next, we analyze the static equilibrium of the body $\mathcal{B}$ in response to τ_{ext} with respect to moments.

$$\begin{aligned} &\sum_{i=1}^{3} \left(R(\theta)\vec{b}_i \right) \times \left(R(\theta) \begin{pmatrix} f_{t,i} \\ f_{n,i} \end{pmatrix} \right) + \tau_{\text{ext}} \\ &\quad = \sum_{i=1}^{3} \left(\vec{b}_i \times \begin{pmatrix} f_{t,i} \\ f_{n,i} \end{pmatrix} \right) + \tau_{\text{ext}} = 0 \end{aligned} \tag{12}$$

Due to the symmetry of the case study, the three normal forces are equal to each other, and the three tangential forces are equal to each other. Taking all three fingers into account, the static equilibrium of $\mathcal{B}$ is given by:

$$\rho f_n + R f_t + \frac{\tau_{\text{ext}}}{3} = 0 \tag{13}$$

Next, we examine the rolling of the disc-fingertip. The rotation of the fingertip-frame relative to the world frame is ψ. The rotation of the fingertip-frame relative to $\mathcal{B}$'s frame is ϕ. The rotation of $\mathcal{B}$'s frame relative to the world frame is θ. Due to the fact that planar rotations are commutative [21], the rotation of the fingertip-frame relative to the world frame is given by:

$$\psi = \phi + \theta \tag{14}$$

So far, we have established five equations (10), (11), (13), (14) (note that (10) is two equations) with six variables $(\theta, f_t, f_n, \rho, \phi, \psi)$. Let us first assume that the finger performs a rolling motion without sliding. In this case, the displacement of

Authorized licensed use limited to: Ben-Gurion University of the Negev. Downloaded on December 03,2023 at 08:12:58 UTC from IEEE Xplore. Restrictions apply.

the fingertip contact along the object boundary is simply:

$$\rho = r\phi \tag{15}$$

Using this equation, we can uniquely determine all six variables for any given τ_{ext}. However, this assumption does not cover the full range of motion. The fingertip will start to slide instead of roll when the tangential force component exceeds its limit. In other words, when the finger contact slides, the contact force lies on the border of the friction cone. Specifically in our case study:

$$f_t = \begin{cases} -\mu f_n & \tau_{\text{ext}} \geq 0 \\ +\mu f_n & \tau_{\text{ext}} < 0 \end{cases} \tag{16}$$

where μ is the coefficient of friction. We can now solve for the six variables for a given τ_{ext}, carefully selecting the correct case sixth equation. We do this by first solving the equations assuming a pure rolling motion (using Eq. (15)). We then check if the result is feasible, by testing if the contact force is within the friction cone: $|f_t| \leq \mu f_n$. If this test is "false," we replace Eq. (15) with Eq. (16) and re-compute.

Using this technique, we can plot the expected displacement of the contact, ρ, as a function of τ_{ext}, for a given coefficient of friction μ. Plots of ρ as a function of τ_{ext} for different values of μ appear in Figure 4 (see Section IV for comparison with experiments). It is evident that until the sliding mode starts, the net displacement ρ is *much lower* than after sliding occurs. Therefore, it may be insightful to understand the relationship between the coefficient of friction and the external torque at which sliding starts. To do this, we treat τ_{ext} as a variable instead of a known parameter, and utilize both Eq. (15) and Eq. (16). The intersection of both equations is the point at which rolling stops and sliding begins, which we call the *slip torque*. This allows us to plot τ_{slip}, the maximal external torque that can be applied before sliding starts, as a function of the coefficient of friction μ. Figure 5 shows, the higher the coefficient of friction, the higher the level of τ_{ext} that would cause the onset of contact sliding. Hence, switching the contacts from frictionless to frictional conditions would not only delay the onset of sliding at the contacts, but also allow the grasping hand to withstand much higher external torques before sliding starts.

III. Design of Dual-Friction Fingertips

In this section we present the design of the rolling dual-friction robotic fingertips. The fingertips have three key features– a locking mechanism, surface normalization, and locking force adjustment. Each of these features are detailed in reason and design.

A. Design Overview

The Rolling robotic fingertip is shown in Fig. 1. It is comprised of the following main parts, which are numbered in the figure. A *roller* (No. 3 in Fig. 1) is a cylinder at the end of the fingertip. The roller is coated in a friction-inducing material (nitrile or latex). This cylinder is free to rotate about its axis, where it is connected to a steel *axle* (No. 6 in Fig. 1) via roller bearings; i.e., the axes of the roller and the axle are always equivalent. The axle is housed in a *swivel mechanism* (No. 2 in Fig. 1), that is primarily cylindrical in shape. The axes of the swivel mechanism and the axle are parallel by default, and coplanar when the locking mechanism is activated. The swivel mechanism is housed within the *base* (No. 1 in Fig. 1), which is also cylindrical in shape. The swivel mechanism and base are connected via needle roller bearings, so that the swivel mechanism is free to rotate within the base; the base and swivel mechanism have equivalent cylinder axes. The *locking surface* (No. 4 in Fig. 1) is a set of rigid teeth that are fixed to the swivel mechanism. The teeth are parallel to the roller by default, at a small distance from it. When locked, the teeth of the locking surface come in contact with the roller and inhibit its ability to freely rotate. Within the swivel mechanism sits the *locking force adjustment mechanism* (No. 5 in Fig. 1), comprised of a spring, a bolt, and two parallel plates.

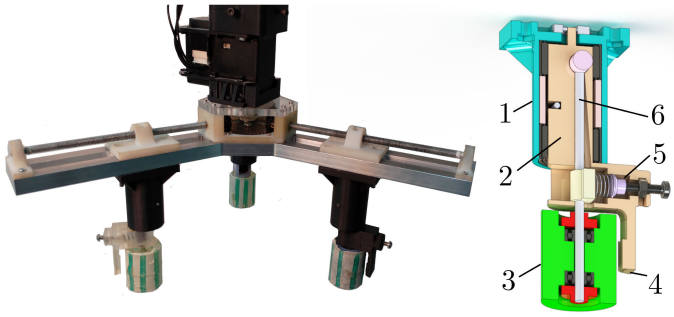

Fig. 1. A section view CAD rendering of the fingertip (right) alongside a picture of a robotic hand with three prototype fingers (left). The main components are enumerated as follows: 1. Base, 2. Swivel Mechanism, 3. Roller, 4. Locking Surface, 5. Locking Force Adjustment System, 6. Axle.

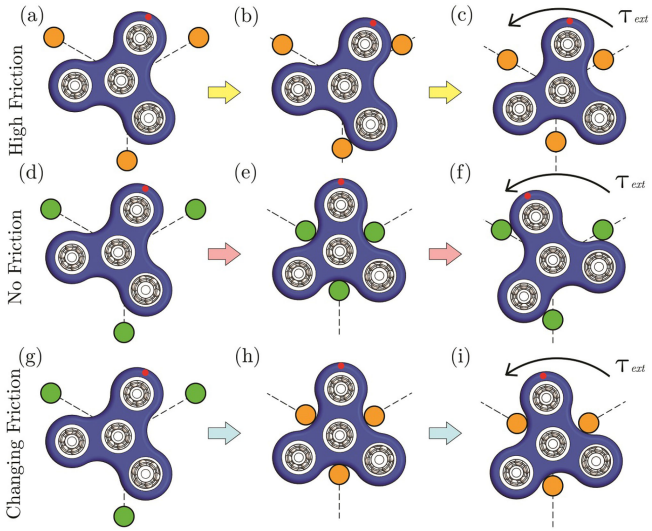

Fig. 2. An illustration of a hypothetical grasping task performed by three types of fingers. The top row shows high-friction fingers (orange), the middle row shows low-friction fingers (green), and the bottom row shows dual-friction fingers (green when frictionless, orange when high-friction). (a) High-friction fingers poised to retract along the dotted lines. (b) The high-friction fingertips reach a two-finger jamming grasp. (c) External torque is applied, the jamming grasp is broken and the object is released. (d) Frictionless fingers poised to retract. (e) Contact sliding causes the object to move until a 3-finger grasp is achieved. (f) External torque is applied, the fingers slide along the object's edges. (g) Dual-friction fingers are poised to retract. (h) While frictionless, the fingers retract and move the object. When a secure 3-finger grasp is achieved, the fingers convert to high-friction contacts. (i) External torque is applied, and the fingers roll-slide along the object's edge to a much lesser degree than the frictionless case. A similar object was grasped in a demonstration available in [18].

Authorized licensed use limited to: Ben-Gurion University of the Negev. Downloaded on December 03,2023 at 08:12:58 UTC from IEEE Xplore. Restrictions apply.

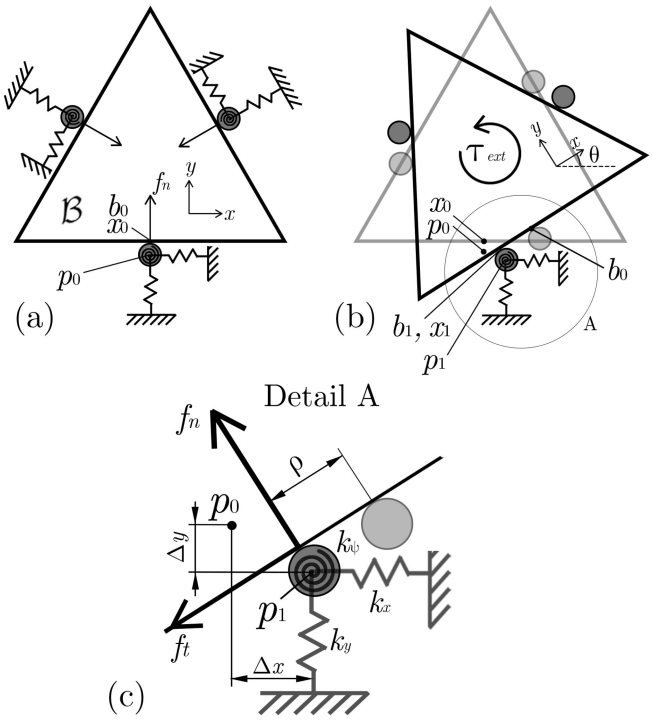

Fig. 3. (a) The triangular object is initially held at three equidistant points by disc-shaped fingers, with compliance modeled for each as mutually orthogonal linear springs and a torsional spring. (b) External torque τ_{ext} is applied to the object, causing it to rotate and compress the springs. (c) An enlargement of (b), showing the notation used.

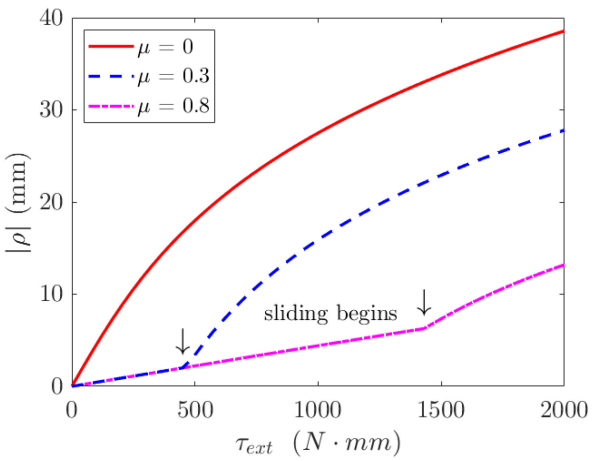

Fig. 4. Finger contact displacement as a function of τ_{ext}. Three degrees of friction are displayed—frictionless, medium friction ($\mu = 0.3$) and high friction ($\mu = 0.8$). When friction exists, there is a critical τ_{ext} where pure rolling stops and sliding begins. The position of this point depends on the coefficient of friction, with significant delay under high friction.

This mechanism is used to adjust the force needed to lock the fingertip.

B. Locking Mechanism

The locking mechanism facilitates the friction change of the fingertip. When the locking mechanism is activated, the fingertip has high friction at the contact point with an object. When the locking mechanism is not activated (default), the fingertip has low friction at the contact point with an object. The locking mechanism is activated by the application of sufficient force– the *locking force*– on the roller.

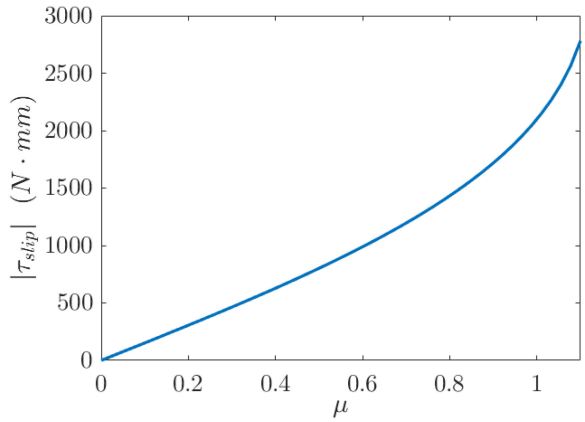

Fig. 5. The critical external torque, $\tau_{\text{ext}} = \tau_{slip}$, as a function of the friction coefficient μ. The higher μ is, the higher τ_{ext} can be applied before sliding begins, and fingertip displacement (ρ) increases dramatically.

While the finger is in its default, low-friction state, the roller is free to rotate about its axis. In this state, when the fingertip contacts an object, it can only apply force normal to the contact point normal. When sufficient normal force is applied to the roller, the spring of the locking force adjustment mechanism compresses, tilting the axle and the roller with it. The roller moves towards the teeth of the locking surface, and wedges into them. The interaction between the roller and the teeth prevents the roller from freely rotating. In this configuration, the roller can apply tangential (friction) forces to an object in contact with it.

C. Surface Normalization

Were the swivel mechanism to be fixed to the base, the locking force magnitude would be dependent on the direction of force application; i.e., a force of a certain magnitude may or may not lock the fingertip, depending on the direction it is applied to the roller. This is because the locking mechanism is activated by pushing the roller against a spring that is housed in the swivel mechanism. If a force is applied in a direction that is not purely parallel to the spring, only the parallel component will work to activate the locking mechanism. This notion can be described by:

$$F_{\text{lock,true}} = \frac{F_{\text{lock}}}{\cos(\gamma)} \tag{17}$$

where γ is the angle between the spring and the force vector. If the minimal locking force magnitude is F_{lock}, the required locking force magnitude will be $F_{\text{lock,true}}$. This characteristic is undesirable, because the locking force threshold would depend on the local contact point geometry. The locking force should ideally have a fixed value, independent of the direction of application– usually the surface normal at the contact point. Therefore, we design the device so that it self-aligns with the object's surface normal.

The swivel mechanism is allowed to freely rotate within the base. The roller and axle are embedded in the swivel mechanism,

Authorized licensed use limited to: Ben-Gurion University of the Negev. Downloaded on December 03,2023 at 08:12:58 UTC from IEEE Xplore. Restrictions apply.

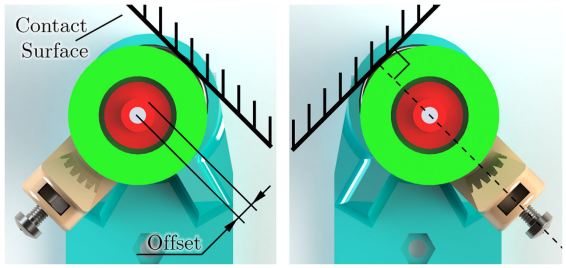

Fig. 6. Typical operation of the surface normalization feature. When the roller contacts an object, the swivel mechanism rotates to align itself with the surface normal.

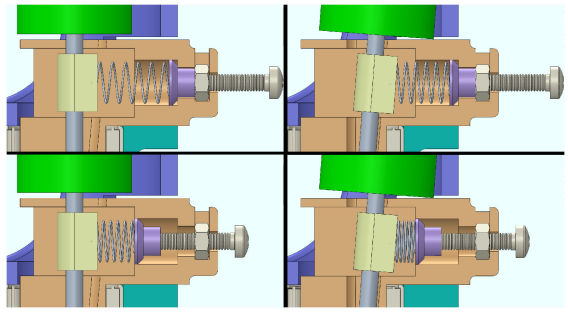

Fig. 7. A rendering of the adjustable locking force mechanism cross section. The mechanism is shown with low pre-compression (top row) and high pre-compression (bottom row), in the default position (left column) and in the locked position (right column).

offset from the swivel mechanism's primary axis. As a result, when a force of arbitrary direction is applied to the roller, it does not typically pass through the swivel mechanism axis. Hence, a torque is applied to the swivel mechanism, causing it to rotate in a direction that minimizes the torque. The offset between the swivel mechanism and roller axes is in the direction of the locking mechanism spring. This directed offset means that when a force is applied to the roller, it causes a torque that rotates the swivel mechanism– and the locking mechanism inside it– normal to the object's surface. Fig. 6 depicts the typical operation of the surface normalization mechanism. This mechanism is not dissimilar to a shopping cart wheel that aligns itself to the direction in which it is pushed. This alignment ideally reduces the angle γ to zero, and eliminates the significance of surface normal direction on the required locking force.

The self-alignment of the locking mechanism to the surface normal can also give us useful information. If we measure the angle of the swivel mechanism relative to the finger base, we can effectively determine the surface normal at the point of contact. To do this, a small, low-torque rotary-potentiometer is fixed to the bottom of the base, with its shaft connected to the swivel mechanism. The potentiometer is used to determine the surface normal direction. This information can be used to determine whether or not an object is being grasped correctly, as demonstrated in a previous work of ours [22]. Alternatively, an unknown object can be probed with the robotic fingertip, thus giving information regarding the object's perimeter (location and surface normal) using low-cost sensors. This too has been demonstrated in previous work [23].

D. Locking Force Adjustment

Different grasping tasks may require different locking force thresholds. For instance, if a lightweight, fragile object is to be grasped, a low locking force threshold is ideal. If the locking force is too high, the object may be damaged before the fingertips are converted to frictional contacts. Conversely, if a heavy, robust object is to be grasped, a higher locking force is needed to ensure proper placement of the fingertips without premature locking. Due to the situational locking force requirements, the locking force magnitude is designed to be easily modified.

If we assume that the angle the roller obtains relative to the swivel mechanism is small when locked, the locking force can be simply defined by Hooke's law: $F_{\text{lock}} = k \cdot \Delta\chi$, where F_{lock} is the force required to lock the mechanism, k is the spring stiffness, and $\Delta\chi$ is the displacement between the default and locked position. This leaves us with a single value of F_{lock} that depends on the spring stiffness and the geometry of the locking mechanism. We enlarge the required locking force by precompressing the spring, so that it applies constant force on the roller that must be overcome to displace it. We then obtain the improved equation for the locking force:

$$F_{\text{lock}} = k \cdot \Delta\chi + F_{\text{preload}} = F_{\text{comp}} + F_{\text{preload}} \tag{18}$$

Where $F_{\text{comp}} = k \cdot \Delta\chi$, and F_{preload} is the pre-loaded force, defined by $F_{\text{preload}} = k \cdot \chi_{\text{precomp}}$. χ_{precomp} is the amount that the spring is compressed for preloading. Changing χ_{precomp} results in the linear adjustment of F_{lock}.

By designing the mechanism so that $\Delta\chi$ is small, we minimize the angle the roller obtains. This maintains compactness of the design while preserving the ability to demand a high locking force. This adjustable force locking mechanism is depicted in Fig. 7, which shows that the value of χ_{precomp} can be changed using a simple nut-and-bolt system to pre-compress the spring.

IV. Experiments

In this section we detail two experiments performed to verify the threoretical analysis, demonstrate the capabilities of the robotic fingertip design, and showcase the advantage of the fingertips. Firstly, we perform an experiment that replicates the conditions of the case study in Section II. An object is grasped by frictionless, and then frictional fingertips, external torque is applied, and the contact location displacement is measured. Secondly, we test the dual-friction fingertip design by verifying that the locking force is truly independent of the force direction. We accomplish this by applying gradually increasing forces on a fingertip at varying angles, and measuring the locking force for each angle. The experiments show the capabilities and advantage of the dual-friction fingertips compared to contemporary fingertips. These capabilities are also demonstrated in an external video accompanying this paper at [18].

A. Torque Resistance With or Without Locking

As a demonstration of the improved grasping capabilities of the dual-friction fingertips, we performed an experiment directly relating to the theoretical analysis in Section II. An equilateral-triangle shaped object was grasped by three fingertips, and torque τ_{ext} was applied to it. The displacement of the fingertips along the object's edge ρ as well as the object's disorientation θ were measured. This experiment was carried out

Authorized licensed use limited to: Ben-Gurion University of the Negev. Downloaded on December 03,2023 at 08:12:58 UTC from IEEE Xplore. Restrictions apply.

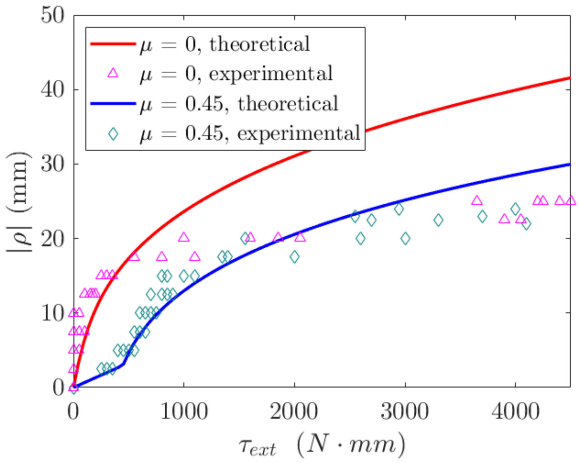

Fig. 8. Theoretical and experimental results of the torque resistance with and without friction at the contact points. Torque was applied to an object and the distance ρ was measured. The frictional case is more robust to torque in this respect, especially for lower torques.

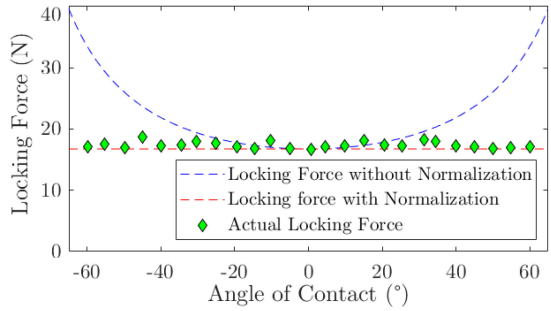

Fig. 9. Experimental results of the surface normalization mechanism. The theoretical force required to activate the locking mechanism, assuming a static swivel mechanism, appears in blue. The theoretical force required to activate the locking mechanism, when the swivel mechanism is allowed to rotate, appears in red. True measured values are displayed as diamonds.

two times– using frictionless fingertips (rolling contacts), and locked dual-friction fingertips. Purely high-friction fingertips were not tested, because the dual-friction fingertips in and of themselves act as high-friction contacts.

The triangular object is set on a flat table with a cylindrical bore at its center. A shaft is rigidly connected to the triangle at its center, and passes through the bore in the table. A torque sensor and applicator are attached to the shaft. In this way, pure torque can be applied to the triangle. The application of torque does not apply force to the triangle, because the shaft is only slightly smaller in diameter than the bore; any force applied to the shaft would be transferred to the table and not the triangle. A robotic hand of our design can close or open the three fingers simultaneously, in an equilateral configuration. We rigidly attached the hand to the table, and used it to grasp the triangular object with any type of fingertip– frictionless, frictional, or dual-friction. The experimental setup and its operation are best viewed in the video accompanying this paper, also available at [24].

An increasing torque τ_{ext} was applied to the triangular object, and the distance between the three initial contact points to the three new contact points was measured. This experiment was done with frictionless and locked dual-friction fingertips– which are essentially high-friction fingertips. In all cases the initial normal force applied to the object was identical. The recorded displacements are shown in Fig. 8. In order to compare our results with the theoretical analysis, all required parameters were measured– $k_x, k_y, k_\psi, f_n^0, \mu$. The analysis is overlayed in the figure. Note that for lower torques there is a good correlation with the theoretical analysis, which diminishes as the torque rises. This is likely due to the non-linearity of the stiffness, which is not taken into account in our model. Naturally, any increase of the stiffness coefficient will result in lower values of ρ, both in the frictionless and high-friction case.

B. Surface Normalization

To test the validity of the surface normalization mechanism described in Section III-C, we performed the following experiment. A rolling dual-friction fingertip was fixed to a rail, and an increasing force was applied to it. The force direction was set at an angle between $(-60°, 60°)$ relative to the locking mechanism. The force was increased until the locking mechanism was engaged, measured by a microswitch placed on the locking surface. The initial and final angles of the swivel mechanism relative to the force were measured by an internal potentiometer. This was repeated for a number of force contact angles, simulating interaction with different surface normals. Fig. 9 shows the experimental results, along with the expected locking force with an ideal swivel mechanism, and without a swivel mechanism. The results clearly indicate that the swivel mechanism effectively eliminates the influence of the surface normal.

V. Conclusion

In this work, we introduce a novel rolling dual-friction robotic fingertip. Convertible friction fingertips can be used to improve grasp robustness or perform in-hand manipulation. The designed fingertips have the unique ability to change from frictionless contacts to frictional contacts by applying force to them. This force can be applied from any direction, and the magnitude required to convert the fingers' state can be adjusted by the user. The capabilities of our fingertips can be seen in a [18]– a video where 15 real-world objects are grasped with the fingertips.

Both low and high-friction gripping contacts are used in industry, but the two are not used in tandem. Frictionless fingertips are good at achieving accurate contact locations, but have a higher tendancy to slide along the object's edge when external wrenches are applied. High friction fingertips are more robust to contact displacement, but are difficult to place accurately, and are susceptible to jamming. Our robotic fingertips allow both of these advantages, without the disadvantages, in one gripping device.

We presented theoretical background and an analytic model of the dual-friction fingertips, showing the expected displacement of the fingertips with or without friction. The model clearly indicates that compared to frictionless contacts, frictional contacts provide superior grasp robustness. In the first experiment presented, we validated the analytic model. A pure torque was applied to an object that is grasped by a hand with three frictionless or frictional fingertips. We measured the displacement of the contact point on the object's surface in each case. For high torques, the advantage of high-friction contacts is not large, and

Authorized licensed use limited to: Ben-Gurion University of the Negev. Downloaded on December 03,2023 at 08:12:58 UTC from IEEE Xplore. Restrictions apply.

the analytic model is not a good predictor of the displacement. This is likely due to the non-linearity of the finger stiffness. For low torques, the results show that the frictional contacts significantly improve the robustness of the grasp in this respect, with good correlation to the analytic model.

In a second experiment, we validated the claim that the force magnitude required to lock the fingertip (converting it to a frictional contact) is independent of the surface normal direction. The results indicate that the finger re-orientation mechanism effectively eliminates the significance of the contact surface normal direction. This means that the fingertips can be used disregarding the surface orientation, knowing that when sufficient normal force is applied, the fingers will convert to frictional contacts.

While cylindrical rolling fingers are suitable for many real-world applications, they essentially work in 2D, which dictates natural limitations. To this end, we have already designed and begun testing dual-friction fingertips with ball rolling element, and an alternative with dual cylinders. These fingertips have the same desired characteristics, such as locking force independence of the fingers in this paper, but in three dimensions. In future work, we will analyze and test these fingertips similarly to this work. Furthermore, we are developing a generalized analytic model of the fingertip. This model will quantify the contribution of friction in grasps using a specialized grasp quality metric.

REFERENCES

[1] A. Bicchi, "Hands for dexterous manipulation and robust grasping: A difficult road toward simplicity," *IEEE Trans. Robot. Autom.*, vol. 16, no. 6, pp. 652–662, Dec. 2000.

[2] A. M. Dollar and R. D. Howe, "The highly adaptive SDM hand: Design and performance evaluation," *Int. J. Robot. Res.*, vol. 29, no. 5, pp. 585–597, 2010.

[3] A. Rodriguez, M. T. Mason, and S. S. Srinivasa, "Manipulation capabilities with simple hands," in *Proc. Exp. Robot.*, 2014, pp. 285–299.

[4] C. H. Xiong, W. R. Chen, B. Y. Sun, M. J. Liu, S. G. Yue, and W. B. Chen, "Design and implementation of an anthropomorphic hand for replicating human grasping functions," *IEEE Trans. Robot.*, vol. 32, no. 3, pp. 652–671, Jun. 2016.

[5] M. R. Cutkosky and P. K. Wright, "Friction, stability and the design of robotic fingers," *Int. J. Robot. Res.*, vol. 5, no. 4, pp. 20–37, 1986.

[6] J. C. Trinkle, J. M. Abel, and R. P. Paul, "An investigation of frictionless enveloping grasping in the plane," *Int. J. Robot. Res.*, vol. 7, no. 3, pp. 33–51, 1988.

[7] E. Rimon and J. W. Burdick, "On force and form closure for multiple finger grasps," in *Proc. IEEE Int. Conf. Robot. Autom.*, 1996, vol. 2, pp. 1795–1800.

[8] M. A. Roa and R. Suárez, "Finding locally optimum force-closure grasps," *Robot. Comput. Integr. Manuf.*, vol. 25, no. 3, pp. 536–544, 2009.

[9] Z. Xue, J. M. Zoellner, and R. Dillmann, "Automatic optimal grasp planning based on found contact points," in *Proc. IEEE/ASME Int. Conf. Adv. Intell. Mechatronics*, 2008, pp. 1053–1058.

[10] R. Suárez, J. Cornella, and M. R. Garzón, *Grasp Quality Measures*. Spain: Institut d'Organització i Control de Sistemes Industrials Barcelona, 2006.

[11] C. Ferrari and J. Canny, "Planning optimal grasps," in *Proc. IEEE Int. Conf. Robot. Autom.*, 1992, pp. 2290–2295.

[12] H. Takeuchi and T. Watanabe, "Development of a multi-fingered robot hand with softness-changeable skin mechanism," in *Proc. Robot.41st Int. Symp. 6th German Conf. Robot.* VDE, 2010, pp. 1–7.

[13] A. J. Spiers, B. Calli, and A. M. Dollar, "Variable-friction finger surfaces to enable within-hand manipulation via gripping and sliding," *IEEE Robot. Autom. Lett.*, vol. 3, no. 4, pp. 4116–4123, Oct. 2018.

[14] Q. Wu, T. G. D. Jimenez, J. Qu, C. Zhao, and X. Liu, "Regulating surface traction of a soft robot through electrostatic adhesion control," in *Proc. IEEE/RSJ Int. Conf. Intell. Robots Syst.*, 2017, pp. 488–493.

[15] D. J. Meyer, M. Wiertlewski, M. A. Peshkin, and J. E. Colgate, "Dynamics of ultrasonic and electrostatic friction modulation for rendering texture on haptic surfaces," in *Proc. IEEE Haptics Symp.*, 2014, pp. 63–67.

[16] Y. Golan, E. Rimon, and A. Shapiro, "Convertible frictionless to frictional fingertips to improve robot grasp robustness," *IEEE Int. Conf. Robot. Autom. Workshop Exploiting Contact Dynamics Manipulation*, Stockholm, Sweden, 2016. [Online]. Available: http://robotics.bgu.ac.il/mw/images/2/24/DualFri.pdf

[17] Y. Golan, A. Shapiro, and E. Rimon, "Convertible frictionless to frictional fingertips for a gripper to improve robotic grasp robustness," Nov. 5 2019, US Patent 10,464,218.

[18] Y. Golan. Dual-Friction Robotic Finger Grasping Demonstrations. (2019, Dec. 31). [Online]. Available: https://youtu.be/zfkFx6ljTlA

[19] E. Rimon and J. W. Burdick, "Mobility of bodies in contact. i. a 2nd-order mobility index for multiple-finger grasps," *IEEE Trans. Robot. Autom.*, vol. 14, no. 5, pp. 696–708, Oct. 1998.

[20] E. Rimon and J. Burdick, "New bounds on the number of frictionless fingers required to immobilize planar objects," *J. Robot. Syst.*, vol. 12, no. 6, pp. 433–451, 1995.

[21] K. Gürlebeck, K. Habetha, and W. Spr̈ßig, *Holomorphic Functions in the Plane and n-Dimensional Space*. Berlin, Germany: Springer Science & Business Media, 2007, Art. no. 10.

[22] Y. Golan, E. Rimon, and A. Shapiro, "Object pose estimation by contact with orientation-sensing robotic fingertips," *IEEE Int. Conf. Robot. Autom. Workshop Robotic Sense Touch*, Singapore, 2017. [Online]. Available: http://robotics.bgu.ac.il/mw/images/c/c8/PoseEst.pdf

[23] Y. Golan, A. Shapiro, and E. Rimon, "Object surface exploration using low-cost rolling robotic fingertips," in *Proc. IEEE Haptics Symp.*, 2018, pp. 89–94.

[24] Y. Golan, A. Shapiro, and E. Rimon. Dual Friction Fingertips experiments and demos. (2019, Dec. 31). [Online]. Available: https://youtu.be/1qG92Gc6z6U

Authorized licensed use limited to: Ben-Gurion University of the Negev. Downloaded on December 03,2023 at 08:12:58 UTC from IEEE Xplore. Restrictions apply.